Chemical doping of MoS$_2$ multilayer by p-toluene sulfonic acid

Shaista Andleeb[1]**, Arun Kumar Singh**[1,2] **and Jonghwa Eom**[1]

[1] Department of Physics and Graphene Research Institute, Sejong University, Seoul 143-747, Korea
[2] Department of Physics, Motilal Nehru National Institute of Technology, Allahabad-211004, India

E-mail: eom@sejong.ac.kr

CrossMark

Abstract

We report the tailoring of the electrical properties of mechanically exfoliated multilayer (ML) molybdenum disulfide (MoS$_2$) by chemical doping. Electrical charge transport and Raman spectroscopy measurements revealed that the p-toluene sulfonic acid (PTSA) imposes n-doping in ML MoS$_2$. The shift of threshold voltage for ML MoS$_2$ transistor was analyzed as a function of reaction time. The threshold voltage shifted toward more negative gate voltages with increasing reaction time, which indicates an n-type doping effect. The shift of the Raman peak positions was also analyzed as a function of reaction time. PTSA treatment improved the field-effect mobility by a factor of ~4 without degrading the electrical characteristics of MoS$_2$ devices.

1. Introduction

Over the last several years, two-dimensional (2D) semiconducting transition-metal dichalcogenide (TMD) has attracted increased research attention because of its emerging electrical and optical properties and great potential in practical applications [1, 2]. Graphene is a representative 2D material that has a conical Dirac spectrum of energy states without a band gap, which results in many interesting physical properties as well as stimulating applications [3–6]. However, the gapless band structure of graphene makes it unsuitable as an electronic material in logic circuits. Molybdenum disulfide (MoS$_2$), a layered TMD, has emerged as a feasible alternative to graphene because it has a moderate energy gap with mechanical flexibility, chemical and thermal stability, and absence of dangling bonds [7–14]. A layer of MoS$_2$ consists of a molybdenum monolayer sandwiched between two sulfur monolayers. The strong intralayer bonds and weak interlayer van der Waals forces make it possible to exfoliate individual MoS$_2$ layers. MoS$_2$ crystals can also be obtained in a large scale by chemical exfoliation and chemical vapor deposition (CVD) techniques [15].

MoS$_2$-based electronic and optoelectronic devices such as field-effect transistors (FETs), integrated circuits, solar cells, photodetectors, memory devices, chemical and biosensors, supercapacitors, and photocatalyzed hydrogen evolution reactors have been successfully fabricated [10, 14–17]. FET is a basic and important application of semiconducting TMD materials. Several issues, including reducing the contact resistance, using different substrates, and depositing high-k materials as the top gate, have been focused on to improve the performance of MoS$_2$ FET [18–22]. Given the ultrathin structure of MoS$_2$ layers, doping of this material has yet to be fully developed. Traditional methods of doping such as ion implantation are not suitable for MoS$_2$ thin layer; hence, alternative approaches, such as chemical and molecular doping, must be explored.

Chemical doping has been used to investigate the surface charge transfer between dopant molecules and MoS$_2$ layer [23]. The charge transfer between dopant and host material modulates the Fermi level and results in the modification of the optical and electrical properties of 2D materials. Chemical doping of MoS$_2$ nanoflakes with solution-based dopants, gases, metal nanoparticles, or self-assembled monolayers has already been reported [24–28]. Mouri *et al* reported the tunable photoluminescence of monolayer MoS$_2$ flakes by n-type and p-type dopants in chemical solution [25]. Fang *et al* reported a degenerate n-doping of MoS$_2$ by potassium metal

ions and the significant change in the electron density of MoS$_2$ nanoflakes [26]. Gold nanoparticles were used by Shi *et al* to effectively decorate MoS$_2$ layers via wet chemical method [27]. They found that gold nanoparticles impose p-doping to the MoS$_2$ transistors. Li *et al* studied the carrier doping of MoS$_2$ nanoflakes by functional self-assembled monolayers with different dipole moments [28]. Our group also demonstrated ultraviolet light-induced reversible and stable charge carrier modulation in single-layer, bilayer and multilayer (ML) MoS$_2$ nanosheets with a combination of N$_2$ and O$_2$ gases [29].

Here, we report the tailoring of the electronic properties of ML MoS$_2$ by p-toluene sulfonic acid (PTSA) molecular doping. PTSA is a well-known dopant for conducting polymers and is highly soluble in water. The charge transport measurements and Raman spectroscopy revealed that PTSA molecule imposes n-doping in ML MoS$_2$. The threshold voltages shifted toward more negative gate voltages after exposure of PTSA molecules for different periods of time, revealing the n-doping in ML MoS$_2$. The charge carrier density and field-effect mobility were also estimated and found to be significantly improved after PTSA treatment. Results indicate that chemical modification is a simple approach to tailor the electrical properties of few-layered MoS$_2$ while maintaining its important electrical characteristics.

2. Experimental details

2.1. Sample preparation

ML MoS$_2$ film was mechanically exfoliated from bulk crystals of molybdenite (SPI Supplies, USA) by the scotch tape method and then transferred to a 300 nm thick highly p-doped SiO$_2$/Si substrate. Optical microscopy, Raman spectroscopy, and atomic force microscopy (AFM) aided in identifying the number of layers of the MoS$_2$ flakes. The ML MoS$_2$ had seven to eight monolayers. Raman spectra were obtained with a Renishaw microspectrometer with 514 nm laser wavelength at room temperature. The laser power was kept at ≈1.0 mW to avoid local heating and defect introduction by the laser.

2.2. Device fabrication and measurements

Photolithography technique was used to make large patterned electrodes (Cr/Au of 6/30 nm thicknesss) for ML MoS$_2$ devices. As the final process, Cr/Au (10/80 nm) ohmic contacts were patterned by e-beam lithography. The channel length of transistors was kept almost same (~2.8 μm) for all devices. The devices were annealed in a tube furnace at 200 °C in a flow of 100 sccm Ar and 10 sccm H$_2$ for 4 h to remove lithography resist residue and minimize the contact resistance of the devices. Electrical characterizations of the devices were performed using Keithley 2400 and Picometer 6485 instruments by two-probe measurements at room temperature in vacuum.

2.3. PTSA doping and characterizations

Electrical charge transport measurements and Raman spectroscopy were used to characterize the pristine ML MoS$_2$ film. The same device was then doped with PTSA for different periods of time, and the effect of PTSA doping was investigated by charge transport measurements and Raman spectroscopy. The PTSA monohydrate (ACS reagent, ⩾98.5%, Aldrich) was dissolved in deionized water to make a PTSA solution with 0.1 M concentration. The ML MoS$_2$ film on the Si/SiO$_2$ substrate was soaked in the PTSA solution for certain periods of time and blow-dried by nitrogen. The sample was then placed in a vacuum desiccator for 1 d to completely dry. The procedure described in our previous papers was followed [30, 31].

3. Results and discussion

Figure 1(a) shows the optical image of ML MoS$_2$ on SiO$_2$ substrate. The fabrication process started with the micromechanical exfoliation of naturally occurring crystals of molybdenite using scotch tape method. The ML MoS$_2$ flakes were then transferred to a 300 nm thick SiO$_2$ substrate with underlying highly p-doped silicon. ML MoS$_2$ was first identified by the contrast in an optical microscope. ML MoS$_2$ was further characterized by Raman spectroscopy and AFM. Figures 1(b) and (c) show the surface morphology and corresponding height profile of the ML MoS$_2$ film using AFM. The thickness of MoS$_2$ is approximately 5.5 nm, which indicates seven to eight layers of MoS$_2$. Figure 1(d) represents the optical image of the ML MoS$_2$ film with Cr/Au electrical contacts. The thickness of the Cr/Au electrical contact is 6 nm/80 nm.

Tailoring the electronic properties of semiconducting channel materials is essential for using these materials in high-performance electronic and optoelectronic devices. Several approaches have been applied to modulate the electronic properties of 2D nanomaterials by depositing dopant atoms, chemical modification by absorption of gas molecules/aromatic compounds, and by surface-induced interstitial doping [32]. In general, interstitial doping is usually difficult to control and often introduces defects, thereby reducing the mobility of host materials. Chemical modification, especially non-covalent functionalization, is one of the most effective methods to tailor the electrical properties of 2D nanomaterials. This type of chemical modification does not change the basic electronic structure and preserves the desired electronic properties of 2D nanomaterials by minimizing the damage to the lattice. In our previous reports, the electronic properties of exfoliated single-layer, bilayer and tri-layer graphene, as well as CVD-grown single-layer graphene, were tailored by PTSA molecular doping without degrading its transparency and electrical properties [30, 31].

Figure 2(a) shows the Raman spectra of ML MoS$_2$ before and after PTSA modification for different periods of time. Two characteristic peaks, E$_{2g}^1$ (in-plane vibration) and A$_{1g}$ (out-of-plane vibration), appear around 384 and 408 cm^{-1},
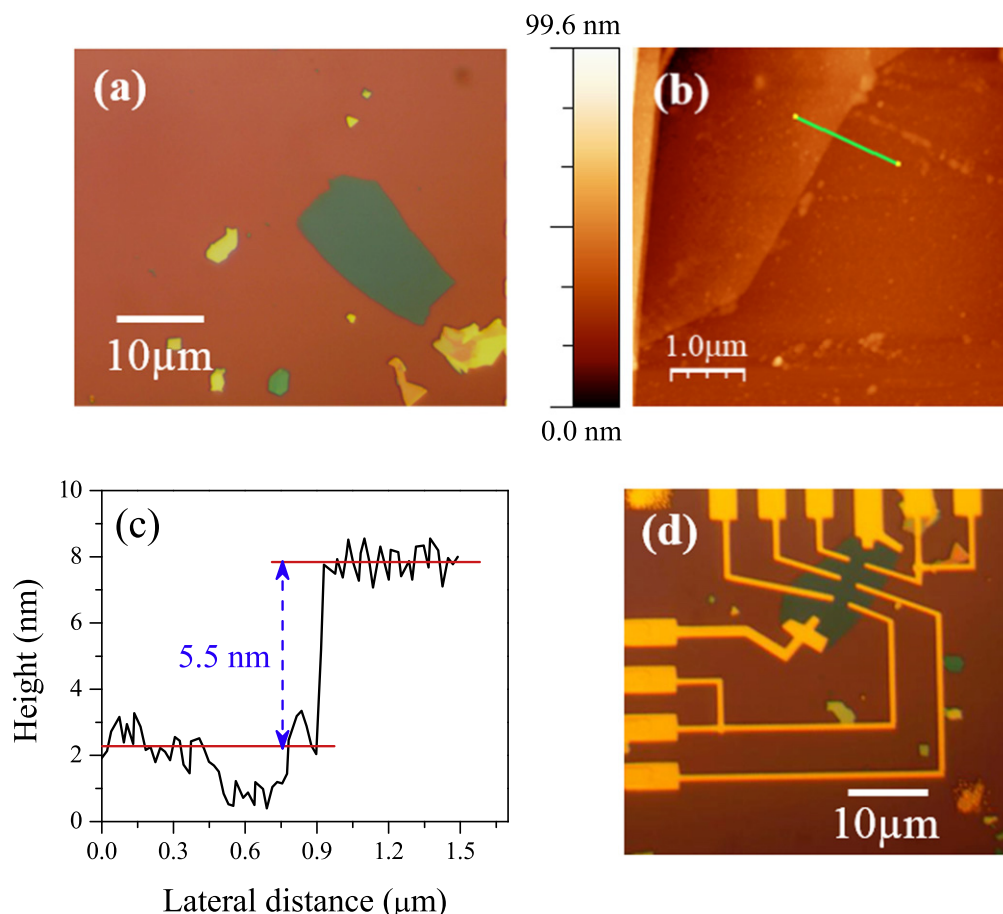
Figure 1. (a) The optical image of mechanically exfoliated ML MoS$_2$ on Si/SiO$_2$ substrate. (b) AFM image of ML MoS$_2$. (c) Height profile measured along the green line in panel (b). (d) Optical image of fabricated device with source and drain electrodes of the transistors made of Cr/Au (6/80 nm).

respectively. The frequency difference between these two Raman modes varies depending on the number of layers and can be easily used as a thickness indicator. The frequency difference between the Raman A$_{1g}$ and E$_{2g}^1$ modes ($\Delta = A_{1g} - E_{2g}^1$) is approximately 24 cm^{-1}, indicating few layers. The Raman spectra of ML MoS$_2$ after PTSA treatment shows downward shifting of the E$_{2g}^1$ and A$_{1g}$ peak positions compared with pristine ML MoS$_2$, as shown in figure 2(a). The downward shifting of the E$_{2g}^1$ and A$_{1g}$ peak positions is attributed to the n-doping of MoS$_2$ as previously reported by others for different systems [33, 34]. The shifting of the E$_{2g}^1$ and A$_{1g}$ peaks toward low wave numbers increases with increasing PTSA exposure time. The n-doping of ML MoS$_2$ is also confirmed by the electrical charge transport measurements.

Figure 2(b) displays the drain current I_{DS} as a function of the applied back-gate voltage V_g at a fixed drain–source voltage, $V_{DS} = 10$ mV, for pristine and PTSA-doped ML MoS$_2$. All electrical characterizations of the devices were performed at room temperature in a vacuum chamber. The $I_{DS}-V_g$ graph reveals an n-type channel for ML MoS$_2$. The I_{DS} shifts toward negative V_g after PTSA treatment. The shift toward the negative gate voltage increases with increasing PTSA exposure time, as shown in figure 2(b). Shifting of the

threshold voltage toward the negative gate voltage reveals the n-doping in the ML MoS$_2$ layers. The same trend is observed on the other devices.

Figure 3(a) illustrates the threshold voltage as a function of PTSA exposure time. The threshold voltage shifts toward the negative gate voltage as the PTSA reaction time increases, revealing the n-doping in MoS$_2$. This chemical doping turns out to be very stable and the same characteristics of the PTSA doped devices have been observed after 10 days in the ambient atmosphere.

Figure 3(b) shows the field-effect mobility of ML MoS$_2$ as a function PTSA reaction time. The mobility of the samples was determined using the relation $\mu = \frac{L}{C_g W V_{DS}}\left(\frac{\partial I_{DS}}{\partial V_g}\right)$, where L is the channel length, W is the channel width, $\left(\frac{\partial I_{DS}}{\partial V_g}\right)$ is the slope of the transfer characteristic of the device in the linear region for particular doping time, and $V_{DS} = 0.01$ V. The length and width of the fabricated device are 2.8 and 9.7 μm, respectively. The gate capacitance C_g for Si/SiO$_2$ is $\sim$115 aF μm^{-2}. The mobility of pristine ML MoS$_2$ was measured as 22.4 cm^2 V^{-1} s^{-1}. The mobility remarkably improved after PTSA treatment, and it was found to be 84 cm^2 V^{-1} s^{-1} after 30 min of exposure to PTSA molecules. The improvement in mobility may be due to reduction of Schottky barrier
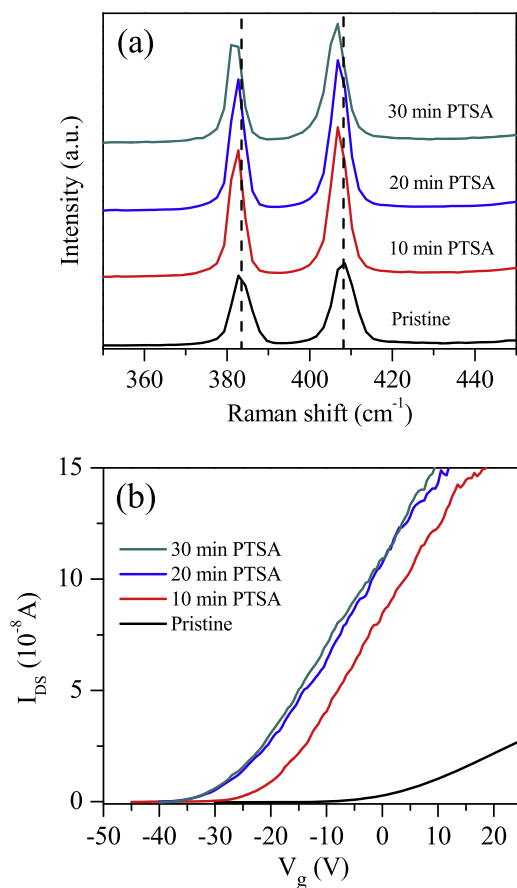
Figure 2. (a) The Raman spectra of ML MoS_2 with 514 nm laser source at room temperature before and after PTSA treatment for different exposure times. (b) Drain–source current as a function of back gate voltage (V_g) for ML MoS_2 before and after PTSA treatment for different exposure times.
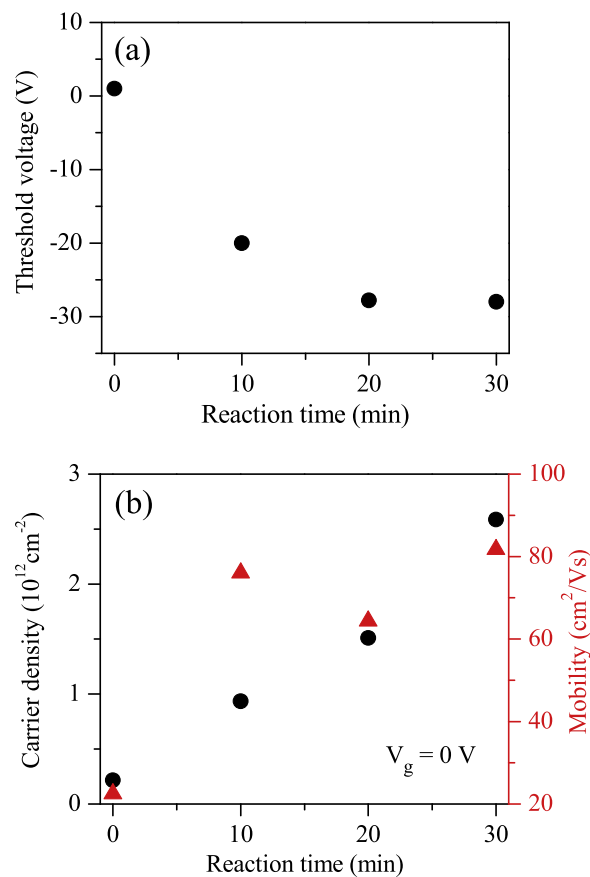

Figure 3. (a) Threshold voltage as a function of the PTSA exposure time of ML MoS_2. (b) Charge carrier density at $V_g = 0$ V and field-effect mobility as a function of the PTSA exposure time of ML MoS_2.

height between source/drain and MoS_2 layers. PTSA increases the electron density in MoS_2 channel, which changes the Fermi level of MoS_2 and lowers the Schottky barrier height between the electrode and MoS_2. Figure 3(b) also shows the charge carrier density (n) of ML MoS_2 as a function of PTSA exposure time at $V_g = 0$ V. Figure 3(b) clearly shows that the charge carrier density of ML MoS_2 significantly changed after different periods of PTSA treatment. The charge carrier densities of our ML MoS_2 transistors were estimated using the relation $n = C_g\left(V_g - V_T\right)/e$, where e is the elementary charge and V_T is the corresponding threshold voltage of the device at different PTSA exposure times.

The n-type doping effect by PTSA solution can be understood as follows. Mo is electropositive in nature as it belongs to 4th transition group of periodic table. The valence electronic configuration of Mo ($5S^1 4d^5$) shows a capacity to accept electrons. On the other hand, SO_3^- has three oxygen atoms, in which two are doubly bonded and the third one is singly bonded with S atom, so there is a resonance in the $[O=S–O]$ bond. SO_3^- can coordinate via monodentate and bidentate moieties owing to the presence of resonance in its structure. The aromatic ring of PTSA contains two groups (CH_3 and SO_3), and SO_3^- is more reactive than CH_3^+. SO_3^-

coordinates with Mo through bidentate mode and shifts electrons to s and d-orbitals of Mo. By accepting the electrons, Mo becomes electron rich and causes n-doping.

4. Conclusions

A simple technique to modulate the electronic properties of ML MoS_2 by PTSA molecular doping was demonstrated. The effect of PTSA doping on the electric properties of ML MoS_2 was investigated by Raman spectroscopy and charge transport measurements. The charge transport and Raman spectroscopy measurements revealed that PTSA molecules impose n-doping in ML MoS_2. The threshold voltage shifted toward more negative gate voltages, thereby confirming n-doping in ML MoS_2. The shift of the Raman peak frequencies was also analyzed as a function of reaction time. Our study demonstrated that molecular n-doping using PTSA is a feasible scheme for improving the electronic properties of MoS_2-based devices.

Acknowledgments

References

[1] Lee C, Yan H, Brus L E, Heinz T F, Hone J and Ryu S 2010 Anomalous lattice vibrations of single- and few-layer MoS$_2$ *ACS Nano* **4** 2695–700

[2] Radisavljevic B, Radenovic A, Brivio J, Giacometti V and Kis A 2011 Single-layer MoS$_2$ transistors *Nat. Nanotechnol.* **6** 147–50

[3] Novoselov K S, Geim A K, Morozov S V, Jiang D, Katsnelson M I, Grigorieva I V, Dubonos S V and Firsov A A 2005 Two-dimensional gas of massless Dirac fermions in graphene *Nature* **438** 197–200

[4] Schwierz F 2010 Graphene transistors *Nat. Nanotechnol.* **5** 487–96

[5] Liao L, Lin Y C, Bao M, Cheng R, Bai J, Liu Y, Qu Y, Wang K L, Huang Y and Duan X 2010 High-speed graphene transistors with a self-aligned nanowire gate *Nature* **467** 305–8

[6] Lin Y M *et al* 2011 Wafer-scale graphene integrated circuit *Science* **332** 1294–7

[7] Xia F, Mueller T, Lin Y M, Valdes-Garcia A and Avouris P 2009 Ultrafast graphene photodetector *Nat. Nanotechnol.* **4** 839–43

[8] Mak K F, Lee C, Hone J, Shan J and Heinz T F 2010 Atomically thin MoS(2): a new direct-gap semiconductor *Phys. Rev. Lett.* **105** 136805

[9] Splendiani A, Sun L, Zhang Y, Li T, Kim J, Chim C Y, Galli G and Wang F 2010 Emerging photoluminescence in monolayer MoS$_2$ *Nano Lett.* **10** 1271–5

[10] Ghatak S, Pal A N and Ghosh A 2011 Nature of electronic states in atomically thin MoS(2) field-effect transistors *ACS Nano* **5** 7707–12

[11] Liu H and Ye P D D 2012 MoS$_2$ dual-gate MOSFET with atomic-layer-deposited Al$_2$O$_3$ as top-gate dielectric *IEEE Electr. Device Lett.* **33** 546–8

[12] Liu H, Gu J J and Ye P D 2012 MoS$_2$ nanoribbon transistors: transition from depletion mode to enhancement mode by channel-width trimming *IEEE Electr. Device Lett.* **33** 1273–5

[13] Jariwala D, Sangwan V K, Late D J, Johns J E, Dravid V P, Marks T J, Lauhon L J and Hersam M C 2013 Band-like transport in high mobility unencapsulated single-layer MoS$_2$ transistors *Appl. Phys. Lett.* **102** 173107

[14] Liu H, Si M, Najmaei S, Neal A T, Du Y, Ajayan P M, Lou J and Ye P D 2013 Statistical study of deep submicron dual-gated field-effect transistors on monolayer chemical vapor deposition molybdenum disulfide films *Nano Lett.* **13** 2640–6

[15] Wang H, Yu L L, Lee Y H, Shi Y M, Hsu A, Chin M L, Li L J, Dubey M, Kong J and Palacios T 2012 Integrated circuits based on bilayer MoS$_2$ transistors *Nano Lett.* **12** 4674–80

[16] Yu T, Lim B and Xia Y 2010 Aqueous-phase synthesis of single-crystal ceria nanosheets *Angew. Chem.* **49** 4484–7

[17] Matte H S, Gomathi A, Manna A K, Late D J, Datta R, Pati S K and Rao C N 2010 MoS$_2$ and WS$_2$ analogues of graphene *Angew. Chem.* **49** 4059–62

[18] Late D J, Liu B, Matte H S, Dravid V P and Rao C N 2012 Hysteresis in single-layer MoS$_2$ field effect transistors *ACS Nano* **6** 5635–41

[19] Wang Q H, Kalantar-Zadeh K, Kis A, Coleman J N and Strano M S 2012 Electronics and optoelectronics of two-dimensional transition metal dichalcogenides *Nat. Nanotechnol.* **7** 699–712

[20] Bertolazzi S, Krasnozhon D and Kis A 2013 Nonvolatile memory cells based on MoS$_2$/graphene heterostructures *ACS Nano* **7** 3246–52

[21] Late D J *et al* 2013 Sensing behavior of atomically thin-layered MoS$_2$ transistors *ACS Nano* **7** 4879–91

[22] Dhakal K P, Duong D L, Lee J, Nam H, Kim M, Kan M, Lee Y H and Kim J 2014 Confocal absorption spectral imaging of MoS$_2$: optical transitions depending on the atomic thickness of intrinsic and chemically doped MoS$_2$ *Nanoscale* **6** 13028–35

[23] Choi M S, Qu D, Lee D, Liu X, Watanabe K, Taniguchi T and Yoo W J 2014 Lateral MoS$_2$ p–n junction formed by chemical doping for use in high-performance optoelectronics *ACS Nano* **8** 9332–40

[24] Kim S *et al* 2012 High-mobility and low-power thin-film transistors based on multilayer MoS$_2$ crystals *Nat. Commun.* **3** 1011

[25] Mouri S, Miyauchi Y and Matsuda K 2013 Tunable photoluminescence of monolayer MoS$_2$ via chemical doping *Nano Lett.* **13** 5944–8

[26] Fang H, Tosun M, Seol G, Chang T C, Takei K, Guo J and Javey A 2013 Degenerate n-doping of few-layer transition metal dichalcogenides by potassium *Nano Lett.* **13** 1991–5

[27] Shi Y, Huang J K, Jin L, Hsu Y T, Yu S F, Li L J and Yang H Y 2013 Selective decoration of Au nanoparticles on monolayer MoS$_2$ single crystals *Sci. Rep.* **3** 1839

[28] Li Y, Xu C Y, Hu P and Zhen L 2013 Carrier control of MoS$_2$ nanoflakes by functional self-assembled monolayers *ACS Nano* **7** 7795–804

[29] Singh A K, Andleeb S, Singh J, Dung H T, Seo Y and Eom J 2014 Ultraviolet-light-induced reversible and stable carrier modulation in MoS$_2$ field-effect transistors *Adv. Funct. Mater.* **24** 7125–32

[30] Singh A K, Ahmad M, Singh V K, Shin K, Seo Y and Eom J 2013 Tailoring the electrical properties of graphene layers by molecular doping *ACS Appl. Mater. Interfaces* **5** 5276–81

[31] Singh A K, Iqbal M W, Singh V K, Iqbal M Z, Lee J H, Chun S H, Shin K and Eom J 2012 Molecular n-doping of chemical vapor deposition grown graphene *J. Mater. Chem.* **22** 15168–74

[32] Han S W *et al* 2011 Band-gap transition induced by interlayer van der Waals interaction in MoS$_2$ *Phys. Rev. B* **84** 045409

[33] Kiriya D, Tosun M, Zhao P, Kang J S and Javey A 2014 Air-stable surface charge transfer doping of MoS(2) by benzyl viologen *J. Am. Chem. Soc.* **136** 7853–6

[34] Yu L *et al* 2014 Graphene/MoS$_2$ hybrid technology for large-scale two-dimensional electronics *Nano Lett.* **14** 3055–63